Process-based Quantification of the Role of Wildfire in Shaping Flood Frequency

Guo Yu[1], Tao Liu[2], Luke A. McGuire[2], Daniel B. Wright[3], Benjamin J. Hatchett[1], Julianne J. Miller[1], Markus Berli[1], Jeremy Giovando[4], Michael Bartles[5], Ian E. Floyd[4]

[1]Division of Hydrologic Sciences, Desert Research Institute, Las Vegas, NV

[2]Department of Geosciences, University of Arizona, Tucson, AZ

[3]Department of Civil and Environmental Engineering, University of Wisconsin-Madison, Madison, WI

[4]Engineer Research and Development Center, U.S. Army Corps of Engineers, Hanover, NH

[5]Hydrologic Engineering Center, U.S. Army Corps of Engineers, Davis, CA

Correspondence to: Guo Yu (guo.yu@dri.edu) and Tao Liu (liutao@arizona.edu)

Abstract

Moderate to high (M-H) severity wildfire can abruptly alter watershed properties and enhance extreme hydrologic responses such as debris flows and floods. The compounding effects of wildfire on flood hazard, represented here via flood frequency analysis (FFA; e.g. 100-year flood) are of growing importance. Standard statistical FFA approaches are ill-suited to examining this issue because wildfire-affected flood peak observations are limited in number and violate the assumption of independent and identically distributed events. Here, we developed a process-based FFA framework that integrates a stochastic rainfall generator, wildfire simulation, inverse modeling, and a physics-based hydrological model to directly simulate the impacts of wildfire on FFA. We applied this framework in the upper Arroyo Seco (uAS) watershed in Southern California, which experienced M-H burn during the 2009 Station Fire. An FFA analysis, performed with simulated peak flows from the first year since fire demonstrates the 100-year flood can be three times larger than simulations that only consider peak flows in non-fire-affected years. On the other hand, coupling process-based FFA with stochastically-simulated wildfire events and watershed's time-varying hydrologic recovery yields "fire continuum FFA", a concept introduced here for the first time. Fire continuum FFA accounts for multiple wildfires within very long synthetic time series. Variability in upper tail flood peaks is substantially higher in fire continuum results as compared with pre-wildfire FFA. This result highlights the importance of wildfire inter-arrival time and post-wildfire recovery processes, both of which are expected to change as a result of climatic change and evolving fire management strategies.

1 Introduction

Wildfire with moderate and high soil burn severity (hereafter referred to as M-H wildfire) abruptly alters hydrologic and soil properties of watersheds by removing vegetation, depositing ash, decreasing infiltration capacity, and changing soil surface structure (e.g., Bowman et al., 2009; Santi et al., 2013; Shakesby, 2011; Shakesby & Doerr, 2006). For example, an ash layer on the soil surface can absorb water rapidly unless it forms an “ash crust” (Balfour et al., 2014; Bodí et al., 2014; Onda et al., 2008), whereas the underlying soil can become water repellent due to a hydrophobic layer of burned organic matter (e.g., DeBano, 1981, 2000; Ebel, 2012; Ebel & Moody, 2013; Moody & Ebel, 2012). Fire can also weaken aggregation of the soil surface, leading to soil crust formation (Albalasmeh et al., 2013; García-Corona et al., 2004; Jian et al., 2018; Larsen et al., 2009; Mataix-Solera et al., 2011). Intense rainfall after wildfire can thus result in substantial overland flow and potential for flash floods and debris flows (e.g., Kean et al., 2016; Liu et al., 2022; McGuire et al., 2017).

This wildfire-flood connection can be understood as a temporally compounding or cascading hazard, in which a particular sequence of events that leads to elevated impacts relative to those same events in isolation (Pescaroli & Alexander, 2015; Zscheischler et al., 2020). Previous empirical studies have focused on quantifying changes in peak flows and sediment yields for the wildfire-affected period, typically the first several years following fire (e.g., Canfield et al., 2005; Chen et al., 2013). After that time, watershed hydrologic and hydraulic properties can recover to the pre-wildfire conditions via vegetation growth, litter deposition, reduction in soil water repellency, recovery of soil surface aggregation and breakdown of fire-induced soil or ash crusts. Studies have shown this recovery time to typically be three to four years, though instances of recovery times up to 30 years have been documented (Kinoshita & Hogue, 2011; Riaño et al., 2002).

Over multidecadal timescales, watersheds can experience multiple wildfires as well as a variety of storms. This can result in floods influenced by and ranging along the "fire continuum"—a concept that emerges from wildland fire science and management that refers to a continuum from pre-wildfire fuel treatments to seasonal wildfire planning to post-wildfire rehabilitation (Hood et al., 2020). We borrowed this idea and defined "fire continuum FFA" herein as a concept of derived flood frequency that accounts for the range of possible flood responses to a continuum of watershed conditions, from pre-wildfire to abrupt perturbation due to wildfire to post-wildfire recovery (Fig. 1). To the best of our knowledge, there is no existing methodological framework for estimating the frequency and severity of flooding along this fire continuum.

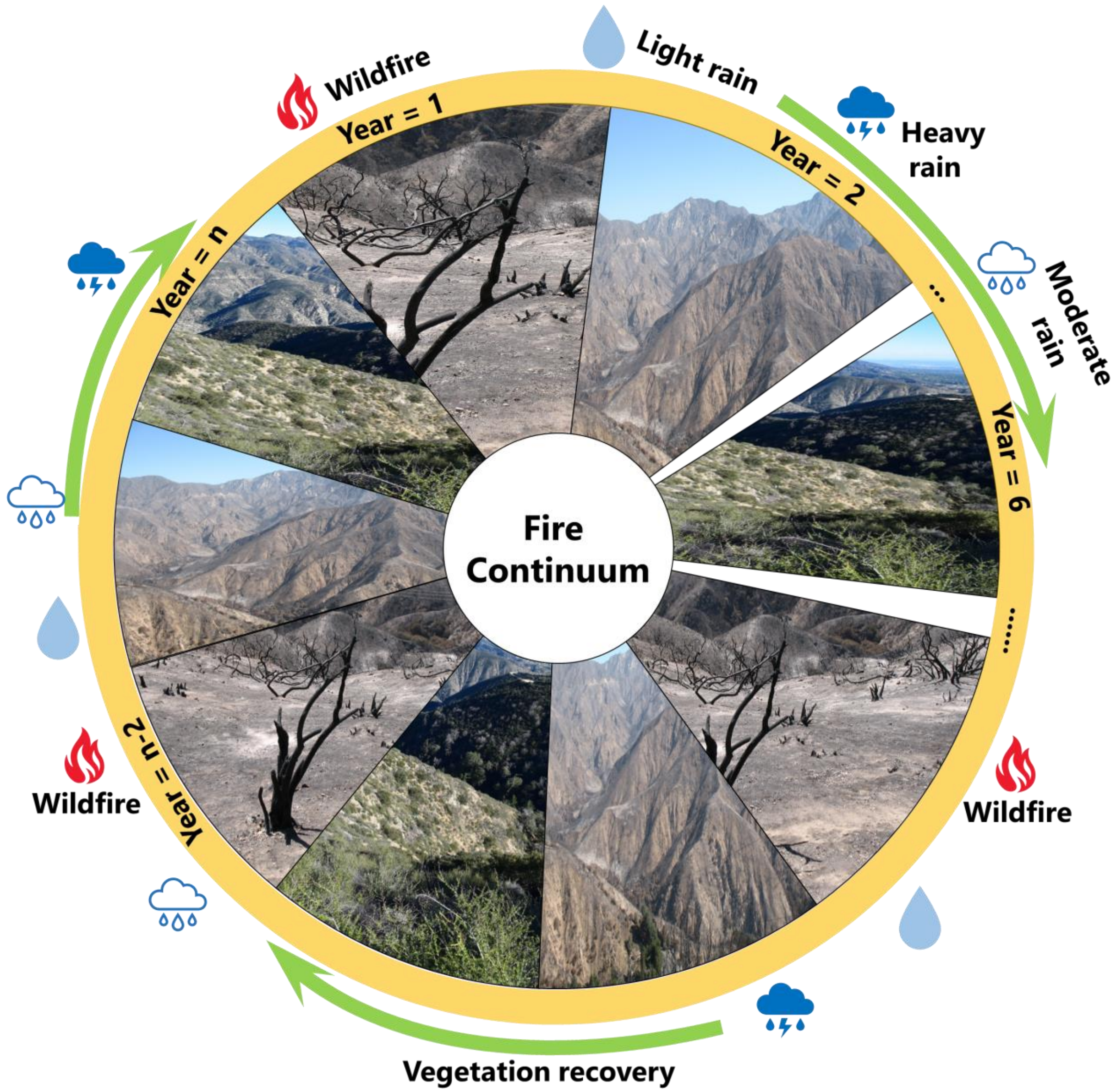

Figure 1. Conceptual schematic for floods occurring along the fire continuum, including the pre-wildfire watershed condition, watershed perturbation due to wildfire, and post-wildfire watershed recovery.

The extent and severity of wildfire is expected to increase in the future, mainly because of fuel accumulation and climate change (Abatzoglou & Williams, 2016; Flannigan et al., 2009; Kitzberger et al., 2007; Westerling et al., 2006). Consequently, watersheds, especially in the western United States (US), are expected to become more vulnerable to the compound wildfire-flood hazards (AghaKouchak et al., 2020; Zscheischler et al., 2020). Therefore, better understanding is needed of how wildfires impact the long-term likelihood and severity of flooding, accounting for the complex interactions of wildfire, vegetation recovery, rainfall, and watershed antecedent conditions (Fig. 1).

The broad family of procedures typically used to assess long-term flood hazards—at least in terms of streamflow—is known as flood frequency analysis (FFA). The goal of FFA is to estimate the annual exceedance probability (AEP) that extreme flows at a particular location along a stream will exceed a given magnitude in a year (e.g., England et al., 2019; NRC, 1988). The reciprocal of AEP is referred to as average recurrence interval (ARI) or the return period (e.g., the 100-year flood). Conventional statistical FFA approaches are poorly suited to estimating wildfire-induced changes in flood frequency for two main reasons. First, flood peaks during the wildfire influenced-period violate the central FFA assumption that flood samples at a given site must be independent and identically distributed (i.i.d.). Because wildfire alters the runoff generating processes of watersheds and because the extent of this alteration depends both on burn severity/extent and time elapsed since the last burn, post-wildfire flood peaks in principle follow a unique distribution and should not be "mixed" with pre-wildfire observations (see Barth et al., 2017; Smith et al., 2011; Yu et al., 2022 for the impacts of other "flood mixtures" on FFA). The violation of i.i.d for post-wildfire flood peaks relates to the second challenge in conventional FFA approaches—limited sample sizes due to relatively long wildfire inter-arrival times. Consider, for example, that 662 of the 1211 (55%) watersheds in the GAGES-II dataset (Falcone, 2011) in the western US have experienced at most one major wildfire event over the past four decades (Yu et al., 2022). This means that wildfire-influenced flood observations will be too few to provide reliable estimates of post-wildfire flood quantiles, especially for upper tail events (e.g., the 100-year flood).

Process-based FFA is a bottom-up alternative to more conventional approaches which provides a different pathway toward quantifying compounding wildfire impacts on flood frequency. It requires simulation of either large numbers of flood events or of time periods long enough to include many such floods (e.g., Lamb et al., 2016; Sivapalan & Samuel, 2009; Yu et al., 2019), typically using some combination of stochastically-generated forcings (e.g., rainfall) and numerical modeling (e.g., rainfall-runoff models to translate these forcings into flood responses). The fundamental aim of process-based FFA is to reconstruct the complex joint relationships among different flood drivers (e.g., rainfall, snowpack, soil moisture, and, in this case, fire impacts on runoff production) via Monte Carlo simulation to produce large simulated flood samples, from which a flood probability distribution can be derived. We have previously developed and applied process-based FFA approaches to understand the impacts of rainfall spatiotemporal structures (Wright et al., 2014; Zhu et al., 2018), different runoff generation processes (Yu et al., 2021), and nonstationary flood seasonality (Yu et al., 2019, 2020) on derived flood frequencies for different watersheds across the US. These previous studies established the core of the fire continuum FFA framework that is used herein.

Process-based approaches are well suited to quantifying the likelihood of compound events because they can represent the causal relationships between multiple drivers and events; this makes it possible to simulate the likelihood of such compound events using the Monte Carlo simulation with a wide range of combinations of driving factors (Zscheischler et al., 2018, 2020). Here, we apply process-based FFA to the upper Arroyo Seco (uAS) watershed in the San Gabriel Mountains, California, which burned primarily at M-H severity during the 2009 Station Fire. Incorporating wildfire impacts requires two new “ingredients” not considered in previous process-based FFA studies: 1) knowledge of the probability of wildfire, and 2) quantitative representation of hydrological impacts of wildfire and its recovery processes. To address the first ingredient, we leverage recent work by the US Forest Service (USFS; Finney et al., 2011; Short et al., 2020), who modeled wildfire occurrence of different severity using fuel type, historical weather data, and simplified fire growth processes (see Section 3.4). To address the second, we use time-varying hydrologic parameters for the uAS watershed developed by Liu et al. (2021) using an inverse modeling approach (Section 3.3).

This study shares some similarities with the recent work in debris-flow modeling which has integrated probabilistic understanding of wildfire occurrence and severity, as well as physical or empirical representations of fire impacts on hydrological and soil hydraulic processes. Kean & Staley (2021) calculated gridded post-wildfire debris flow susceptibility over a 40,000 km^2 area across southern California as a product of historical mean annual probability of wildfire and rainfall recurrence intervals from the National Oceanic and Atmospheric Administration (NOAA) Atlas 14 (Perica et al., 2014). Thomas et al. (2021) developed a framework for investigating the changing probability of debris flows throughout post-fire recovery but not over the full fire continuum. These studies emphasize the need for additional work on cascading rainfall-induced hazards following fire, particularly in southern CA (e.g., Doehring, 1968; Eaton, 1936; J.W. Kean et al., 2019).

We add to these prior studies but focus instead on flood frequency and leverage physics-based wildfire simulations to provide estimates of burn probabilities. We also develop a flexible framework to estimate flood frequencies for both post-wildfire conditions and the fire continuum (i.e., probabilistic estimation; Fig. 1). For the post-wildfire condition, we designed a deterministic experiment that can simulate flood frequency as a function of time after wildfire and percentage of burn area. For the fire continuum, we stochastically combine wildfire occurrence, rainfall intensity, and antecedent watershed conditions to produce a large number of hypothetical flood simulations, which allow us to study wildfire impacts on long-term annual flood recurrence intervals, subject to certain limitations described later. We demonstrate the potential of process-based FFA in wildfire-prone watersheds and underscore the importance of interdisciplinary collaboration among wildfire scientists, soil physicists, and hydrologists to understand this complex and little-understood cascading hazard. To the best of our knowledge, this work represents the first study to utilize a process-based approach to incorporate the hydrologic impacts of and recovery from wildfire into FFA at a watershed scale.

2 Study Area

The 42 km^2 uAS watershed is located in the San Gabriel Mountains above the US Geological Survey (USGS) stream gage near Pasadena, California (gage ID: 1109800) (Fig. 2). It is quite steep, with elevation ranging from 400 to 1900 meters above sea level and an average slope of 30° (Kean et al., 2011). Soils are coarse textured (e.g., sandy loam) and shallow with partial exposure of bedrock. The uAS watershed is situated in the NOAA South Coast climate division (Guttman & Quayle, 1996; hereafter referred to as South Coast), which has a semi-arid Mediterranean climate, with moderately wet winters and dry summers. Based on the Landfire 2020 data (Rollins, 2009), the vegetation type across the South Coast, including the uAS watershed, is predominantly shrub, conifer, and hardwood (Fig. 2c and 2d).

Because of the dry climate and abundant fuel, the area is susceptible to seasonal wildfires as shown by observed burn extents (Fig. 2a). Between late August and mid-October 2009, the Station Fire affected the Angeles National Forest in Los Angeles County, resulting in approximately 82% of the uAS watershed being burned at moderate and high (M-H) soil burn severity (Fig. 2b).

According to the California Department of Forestry and Fire Protection, more than half of the watershed area has previously burned twice, in 1896 (unnamed fire) and in 1959 (Woodwardia Fire on October 14th). Based on the nature of the chaparral ecosystem that is characterized by a crown fire, these fires are assumed to burn at similar patterns of M-H severity as the Station Fire (e.g., Haas et al., 2016; Krammes, 1960).

Runoff in unburned areas of the San Gabriel Mountains is a combination of infiltration (Hortonian)- and saturation-excess (Dunne) overland flow and lateral subsurface flow (Doehring, 1968; Valeron & Meixner, 2009). After wildfires, however, the reduction in litter and canopy cover along with lower effective infiltration rates (i.e., basin-averaged infiltration rate) promote infiltration excess overland flow, leading to rapid runoff generation in response to even modest rainfall intensities (Liu et al., 2021, 2022; Schmidt et al., 2011).

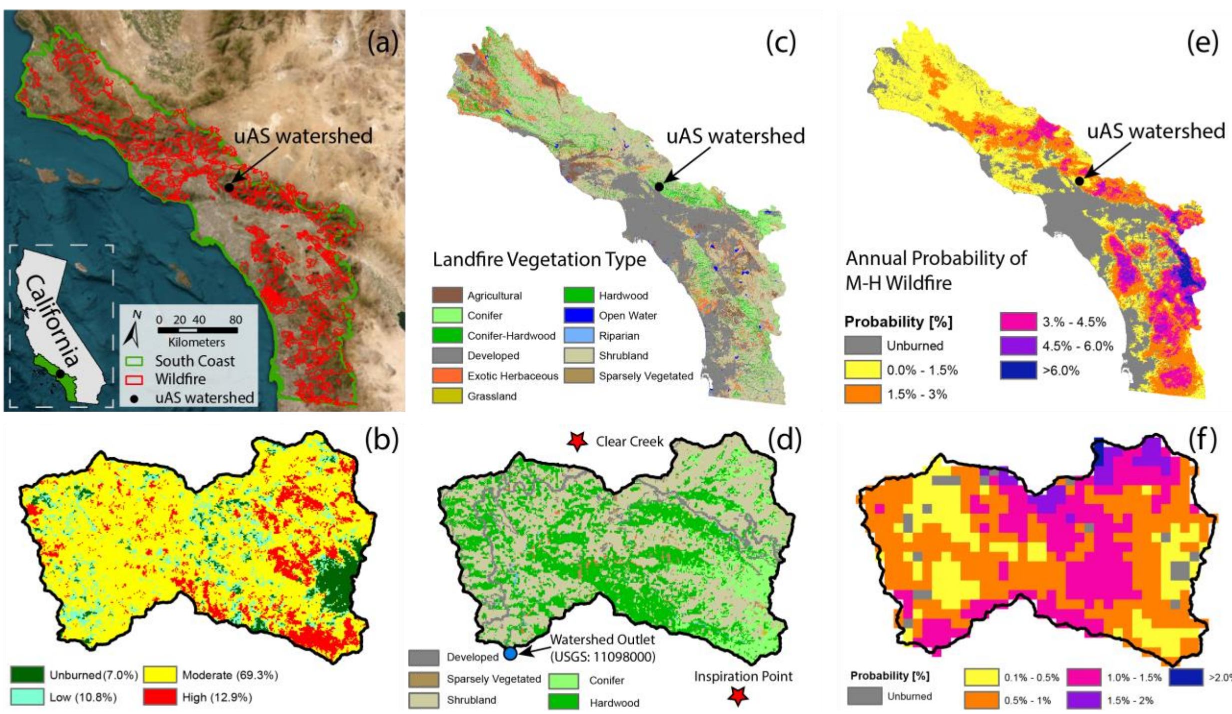

Figure 2. (a) Locations of uAS watershed and South Coast NOAA climate division and spatial distribution of the Monitoring Trends and Burn Severity (MTBS; Finco et al., 2012) wildfire perimeters for the 1984-2021 period. Inset map in (a) shows the relative location of uAS watershed and South Coast with respect to California. (b) The burn severity for the uAS watershed after the 2009 Station fire. The spatial distribution of Landfire vegetation type and

USFS simulated burn probability for the (c; e) South Coast and (d; f) uAS watershed, respectively. The watershed outlet and Clear Creek and Inspiration Point rain gages are shown in (d).

3 Data and Methods

In this section, we provide a detailed description of the multiple data sources and the methods used in this study. Our process-based FFA approach is a modularized framework whose overall functionality is divided into separate components (Fig. 3)

3.1 Data

Precipitation observations were obtained from two tipping bucket rain gages near the uAS watershed (Fig. 2d). These were aggregated into 15-min resolution timeseries. The Clear Creek gage has a longer and more complete record than the Inspiration Point gage; the former was used for October 2000-September 2021 except for a gap from October 2001 to September 2002, during which observations were used from the Inspiration Point gage. (For overlapping periods between gages, their rainfall values have a Spearman's rank correlation of 0.93 with $p < 0.001$.) Rainfall is assumed to be uniform over the watershed, which is defensible given the high correlation between two rain gages and small watershed size. These rainfall observations were used for calibrating both the stochastic rainfall generator (Section 3.2.1) and rainfall-runoff model (Section 3.2.3). Continuous streamflow measurements from the USGS were used for rainfall-runoff model calibration, while USGS annual peak flows were used for comparison against process-based FFA results.

To understand the probability of M-H wildfire occurrence in the watershed, data on burn probability and conditional probability of flame-length exceeding four feet (i.e., M-H fire intensity) were obtained from the USFS (Short et al., 2020; Fig. 2e and 2f). This dataset was generated by using the geospatial Fire Simulation model (FSim; Finney et al., 2011), which includes modules for weather generation, wildfire occurrence, fire growth, and fire suppression. Short et al. (2020) simulated the occurrence and growth of wildfires for more than 10,000 hypothetical present-climate fire seasons to estimate burn probabilities at 270-m resolution across the US.

3.2 Process-based FFA

Our process-based FFA approach involves the Complete Stochastic Modelling Solution stochastic rainfall generator (CoSMoS; Papalexiou, 2018; Papalexiou et al., 2020), simulated soil moisture from the Noah land-surface model forced by the Phase 2 of the North American Land Data

Assimilation System forcings (referred to as NLDAS-Noah; Xia et al., 2012), and the event-based K2 hydrological model (Goodrich et al., 2012; Fig. 3).

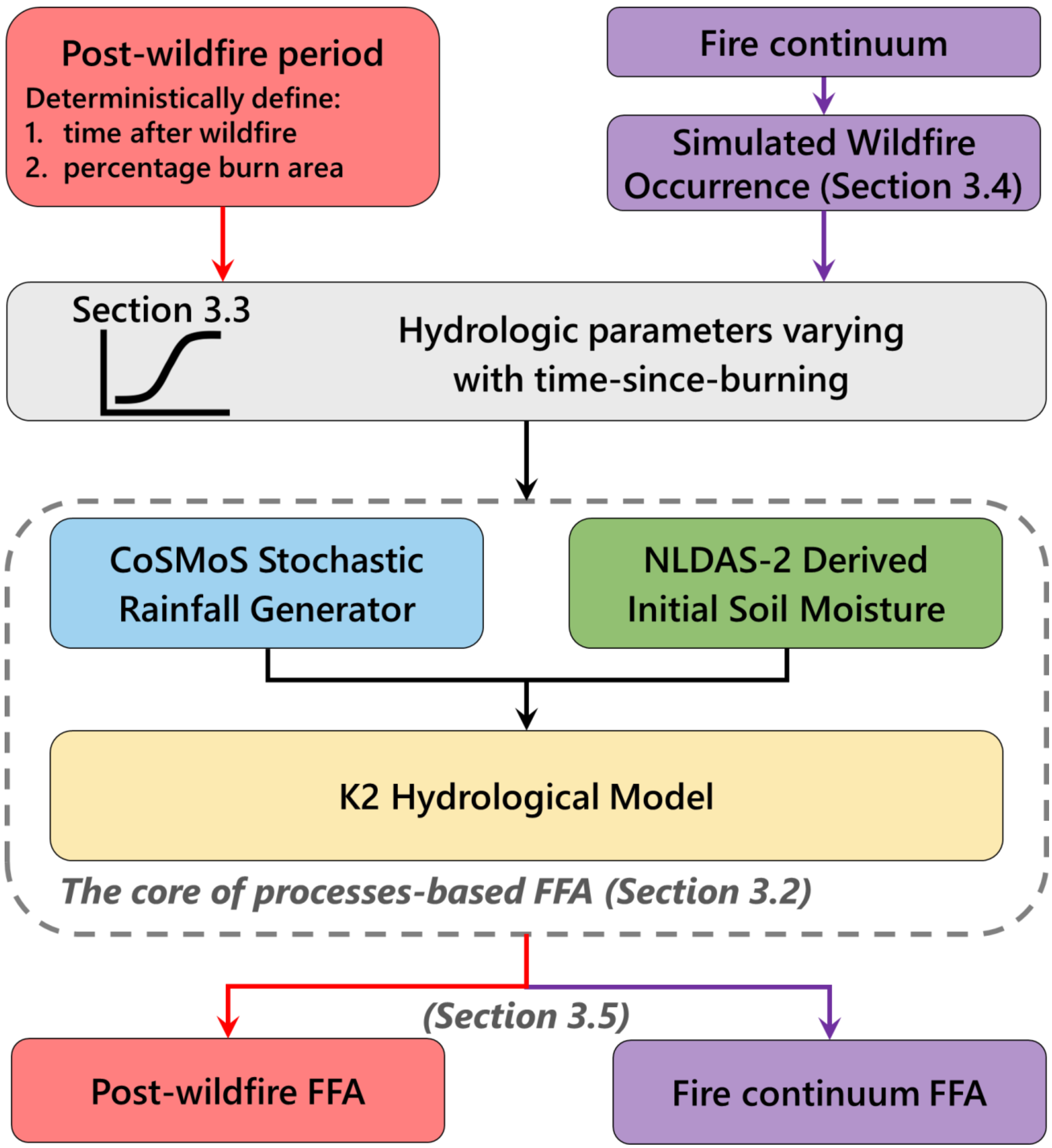

Figure 3. Flowchart of process-based framework for post-wildfire and fire continuum FFA.

3.2.1 CoSMoS

CoSMoS is an R-based tool for stochastically simulating univariate and multivariate non-Gaussian time series. It can reproduce marginal distributions, intermittency, and cross- and auto-correlation structures of various hydrometeorological variables (Papalexiou, 2018). Here, we fit CoSMoS to 21 years of gage-based rainfall observations to determine the marginal distribution, autocorrelation structure, and dry-period distribution of 15-minute rainfall for each month of the year (see Fig. S1-S2 for the fitted distributions for rainfall intensities and autocorrelation structures, respectively). CoSMoS is then used to generate long-term (e.g., 500 synthetic years) continuous 15-minute synthetic rainfall timeseries. Based on the estimated time of concentration for the uAS watershed (Liu et al., 2021), the largest 12-h rainfall accumulations from each synthetic year were selected as annual rainfall maximum and were used to force the K2 hydrological model to simulate the annual streamflows maxima. Thus, we assume annual maximum precipitation drives the annual maximum flood.

3.2.2 Antecedent Soil Moisture

The K2 hydrological model is event-based and requires antecedent volumetric moisture conditions for initialization. We used the NLDAS-Noah simulated top-layer (0-10 cm) volumetric soil moisture for the single NDLAS grid that encompasses the uAS watershed. For each day of the year (i.e., 1 to 365), we fit a normal distribution to the NLDAS-Noah simulated daily mean soil moisture for the 1979-2021 period. When performing an event-based hydrological simulation, the initial soil moisture is randomly generated using the fitted parameters based on the day of the year when the CoSMoS simulated annual maximum rainfall occurs (Fig. S3). This pairing approach ensures both realistic seasonality and interannual variability in watershed conditions.

3.2.3 K2 Hydrological Model, Flood Simulation and Derived FFA

K2 is a spatially distributed, physics-based model designed for simulating event-based rainfall-runoff processes in small-to-medium watersheds. It conceptualizes a watershed as a cascade of hillslopes and channels and simultaneously represents interception, infiltration, and surface runoff on the hillslope as well as flow routing and transmission losses in the river channels (Goodrich et al., 2012; Smith et al., 1995). Liu et al. (2021) set up a K2 model for the uAS watershed with 1,289 hillslope and 519 channel elements; the same model setup was used for this study. Liu et al. (2021) performed sensitivity analyses of K2 model parameters and identified hillslope saturated hydraulic conductivity (K_{sh}) and channel roughness (n_c) to be the most sensitive parameters to streamflow. K_{sh} and channel roughness, n_c, were further automatically calibrated for both pre- and post-wildfire conditions using the Progressive Latin Hypercube Sampling scheme, which systematically generates representative samples while ensuring coverage of the entire parameter space in a progressive manner (Sheikholeslami & Razavi, 2017).

While K2 is designed to simulate infiltration-excess overland flow, floods in the San Gabriel Mountains have been associated with a combination of infiltration-excess and saturation-excess runoff-generation mechanisms. Here, we use K2 to estimate peak flows rather than details of flood dynamics, runoff-generation, or flow volume. We assume that K2 can provide a reasonable estimate of annual flood peaks (i.e., high flow events in which infiltration-excess flow will be presented). See Fig. S4a for the Kling-Gupta Efficiency (KGE) values for the simulated 11 historical flood events using the top 100 parameter sets.

Coupling the calibrated K2 model with a CoSMoS-simulated annual rainfall maximum (Section 3.2.1) and a seasonally-realistic watershed antecedent soil moisture (Section 3.2.2) yields a synthetic annual peak flow maxima. We repeat this procedure *n* times to create one realization of

n synthetic years of annual maximum flows. These are then ranked in descending magnitude. The AEP of each streamflow maxima is calculated by dividing its rank by the total number of simulated annual maximum flows. For example, the AEP for the largest flood event if $n = 500$ is 0.02 and its ARI is 500-year.

3.3 Inverse Modeling Approach for Quantifying Hydrological Impacts of Wildfire

Inverse modeling approaches have been used for quantifying changes in hydrologic and soil properties after wildfires at watershed scales (e.g., Chen et al., 2013; Ebel & Martin, 2017; Liu et al., 2021; Shakesby et al., 1993). Such approaches typically involve two steps: 1) calibrating the relevant model parameters against streamflow observations for several post-wildfire storm events, and 2) fitting a curve to the calibrated model parameters with respect to time after wildfire. Liu et al. (2021) used such an approach to demonstrate that K_{sh} and n_c are the most sensitive and physically reasonable parameters for controlling the post-wildfire hydrologic processes in K2 for the uAS watershed. This is supported by other work showing that runoff generating mechanisms for burned watersheds are typically Hortonian (Schmidt et al., 2011) and thus sensitive to the saturated hydraulic conductivity of the near-surface (McGuire et al., 2018). Additionally, hydraulic roughness in channels is expected to decrease following fire in the uAS because observations suggest that fine grained post-wildfire dry ravel deposits likely obscure channel boulders (DiBiase & Lamb, 2019; Florsheim et al., 2017; M. P. Lamb et al., 2011; Tang et al., 2019).

Liu et al. (2021) auto-calibrated K_{sh} and n_c in K2 simulations for three pre-wildfire events from 2000 to 2008 and eight post-wildfire events ranging from <1 to 10 years after the 2009 Station Fire. For each event, the top 100 best-fit parameters sets out of 2,500 simulations were retained for fitting logistic regressions to quantify their temporal changes. These parameter sets exhibit KGE values mostly ranging between 0.6 and 0.8 (Fig. S4a). The best-fit model parameter set result in the “best” logistic regression, whereas the top-100 values provide an ensemble of regressions representing the uncertainty in the parameters (Fig. S4).

3.4 Modeling M-H Wildfire Probability

Because the temporal changes in model parameters derived by Liu et al. (2021) were primarily driven by M-H soil burn severity (e.g., Fig. 2b), it was necessary to estimate the annual occurrence probability of M-H severity burn conditions. Fire intensity, represented by the amount of energy released by a burning fuel, is highly correlated with soil burn severity, especially in forested landscapes of southern California (Keeley, 2009). In forested landscapes, like the San Gabriel Mountains, high fire intensity will result in crown fire, which typically causes spread of wildfire and high levels of vegetation consumption and mortality (Alexander et al., 2011; Scott, 2005). Therefore, high-intensity crown fire is a useful proxy for moderate-high burn severity. We thus assumed an equivalent relationship between fire intensity and soil burn severity in this study; this assumption has been previously applied in both research (Haas et al., 2016; Tillery et al., 2014; Tillery & Haas, 2016) and practice (Napoli et al., 2022; Scott et al., 2020).

We calculated the annual probability of M-H wildfire by multiplying burn probability and the conditional probability of M-H fire intensity (Fig. 2e and 2f). The basin-averaged probability of M-H wildfire for the uAS watershed is 0.00862, corresponding to 116 years of wildfire inter-arrival time (Fig. 2f). To quantify the uncertainty of M-H wildfire probability for the uAS watershed, we leveraged a spatial bootstrap technique and regional estimates of M-H wildfire burn probability. Specifically, we repeatedly uniformly transposed the uAS watershed outline to other non-developed areas within the South Coast homogenous wildfire regime region to calculate a new probability; repeating this procedure a large number of times can provide an estimate of uncertainty in the probability of M-H wildfire for the uAS watershed. Furthermore, the distribution of USFS-derived fire size for the South Coast shows that simulated fire sizes are typically much larger than the 42 km^2 size of uAS watershed (Finney et al., 2011). Therefore, it is reasonable to assume that the probability of M-H fire that we derive here is a probability associated with burning the entire watershed. We make this assumption in our fire continuum FFA, but also explore the impact of partially burning the watershed in the post-wildfire FFA. (We were unsuccessful in obtaining the fire size distribution from the USFS and thus were unable to consider it probabilistically.)

3.5 Post-wildfire and Fire Continuum FFA

In this study, we distinguish between post-wildfire and fire continuum FFA: the former refers to flood frequencies for the relatively short post-fire period in which hydrologic processes are most affected, whereas the latter refers to long-term flood frequency that considers both post-fire recovery and less hydrologically dynamic pre-fire periods. Post-wildfire FFA were used to estimate the changes in flood frequencies with respect to different percentage burn area and time after wildfire. On the other hand, fire continuum FFA reflects the underlying flood frequency stemming from hydroclimatologic and wildfire variability, including fire occurrence and watershed recovery.

3.5.1 Post-wildfire FFA

Here, we used deterministic numerical experiments to quantify the changes in FFA as a function of time after wildfire and percentage burn area. We designed 20 scenarios to represent 20 different combinations of percentage burn area and time after wildfire. The results of these experiments are referred to as post-wildfire FFA (Fig. 3). Experiments considered different burn area percentages by randomly selecting contiguous hillslopes, which total percentage area exceeds the threshold: 20%, 40%, 60%, 80%, and 100%. The average historical time between fire occurrence and the next heavy rainfall is 47 days and is tied to the seasonality of precipitation in the region; this interval was used to approximate the 'within 1 year' post-wildfire FFA time horizon." Additional horizons of 2, 3, and 4 years after the wildfire were also modeled. In each scenario, we ran 10 ensemble members of 500 synthetic annual maximum flood simulations each, with the ensemble reflecting stochastic uncertainties in rainfall intensities, antecedent soil moisture, model parameters, and randomly-selected locations of burn area.

3.5.2 Fire Continuum FFA

Fire Continuum (stochastic) FFA was used to resolve the impacts of the joint variabilities of rainfall, soil moisture, wildfire impact, and post-wildfire recovery on flood frequency. We derived annual rainfall maxima and associated antecedent soil moisture for 500 synthetic years, during which wildfire occurrence (i.e., inter-arrival time) is modeled using regional wildfire probabilities (Fig. 2e) and a spatial bootstrap scheme (Section 3.4). As mentioned in Section 3.4, we were forced to assume that the entire watershed is burned due to lack of supporting data. Between two wildfire events, K_{sh} and n_c are spatially uniform and are functions of time since fire (Section 3.3). The resulting 500 simulated annual peak flows yield one ensemble member; 100 such ensembles of 500 peak flows each were conducted for a total of 50,000 simulated peak flows.

4 Results

4.1 Historical Floods and Pre-wildfire FFA

Process-based estimates of flood frequency for the uAS watershed under pre-wildfire conditions are compared with 1914–2021 USGS observed annual peak flows (Fig. 4a). The four post-wildfire flood peak observations vary over two orders of magnitude (131 m^3 s^{-1} for one year after to <1 m^3 s^{-1} four years after) and have ARIs that decrease from 20-year (AEP=0.05) to ~1-year (AEP≈1.0) from one to four years after the 2009 Station Fire (Fig. 4a). This points to the role of watershed recovery in counteracting the wildfire impacts on flooding, given that maximum hourly rainfall intensities associated with post-wildfire floods exhibit smaller differences (Fig. 4b). Process-based flood frequency curves agree well with observed peak flows for $ARI \geq 3$-year—i.e., the magnitudes of floods that are important for most flood management applications—but underestimate for $ARI < 3$-year (Fig. 4a). Differences between simulated FFA and USGS observations for the small ARI can be associated with two factors: (1) small flood events can be driven by variables other than annual maximum rainfall, such as long duration, low intensity rainfall; (2) small floods can be driven by subsurface flow, which is not well represented by the K2 model (Canfield et al., 2005; Goodrich et al., 2012; Liu et al., 2021).

Recent observations demonstrate that debris flows and extreme floods across the San Gabriel Mountains are associated with high intensity, short duration rainfall events following wildfire (e.g., Liu et al., 2022; Oakley et al., 2018). More generally, observed flood peaks for the 1979-2021 period and their associated maximum hourly rainfall intensities are strongly correlated, with a Spearman rank correlation $\rho_s = 0.69$ ($p = 0.0005$; Fig. 4b). Similarly, the maximum 15-min rainfall intensity also correlates with observed flood peaks for the 2000-2021 period ($\rho_s = 0.65$; $p = 0.0057$), when rain gauge data are available. Regardless of wildfire, there is high variability in peak flows with respect to the maximum hourly rainfall intensity (Fig. 4b). For instance, storms with a maximum hourly rainfall intensity of ~15 mm h^{-1} can lead to flood peaks ranging from 10 to 100 $m^3 s^{-1}$ (Fig. 4b).

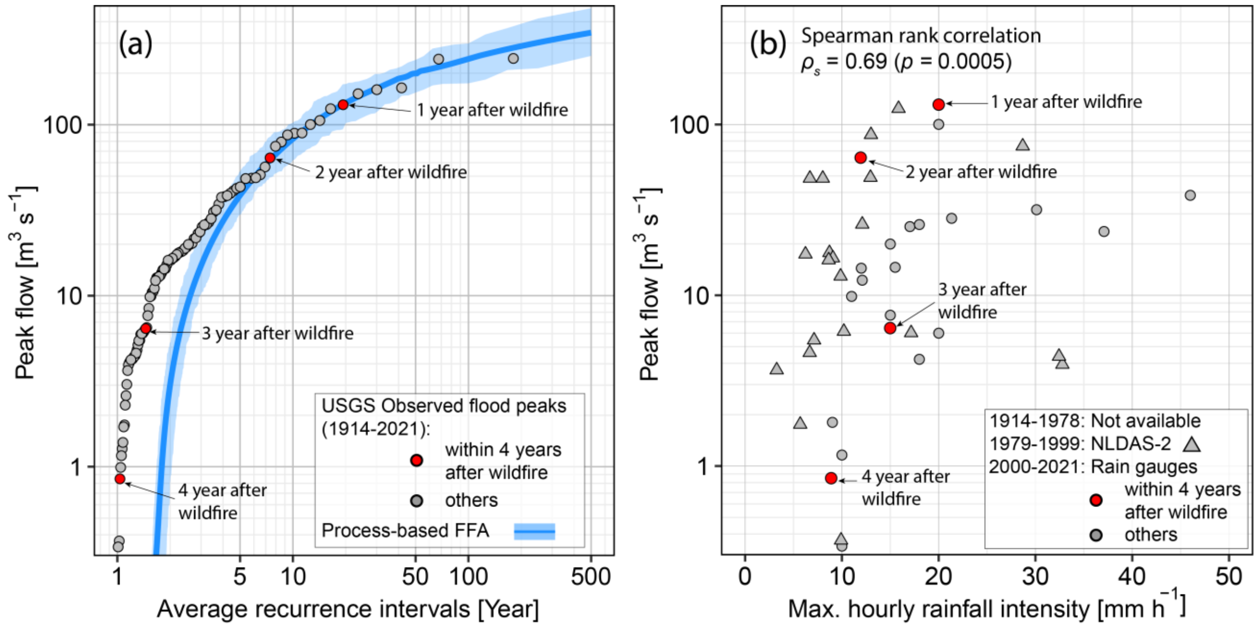

Figure 4. (a) Process-based FFA for pre-wildfire conditions as well as observed flood peaks plotted using Cunnane plotting positions (Cunnane, 1978). (b) USGS observed flood peaks and their corresponding NLDAS-2- (1979-1999) and gauge-based (2000-2021) hourly rainfall intensities. Blue line and shade in (a) represent the mean and range of derived frequencies from 100 ensemble members. Flood peaks within four years after the 2009 Station fire are highlighted in red on both panels.

To further understand the variability in flood peaks with respect to their dominant drivers, we leverage the process-based flood simulation that facilitates understanding how different physical drivers interact to produce floods (Fig. 5). First, maximum hourly rainfall intensities play a first-order role in driving the peak flows. Flood magnitudes increase substantially from < 10 $m^3 s^{-1}$ to a range between 100-year (241 $m^3 s^{-1}$) to 500-year (345 $m^3 s^{-1}$) floods, as rainfall intensities increase from 10 to 100 mm h^{-1} (Fig. 5). Second, high soil moisture can enhance flood magnitudes regardless of rainfall intensity, mainly for floods less than 20-year ARI (Fig. 5a). However, high rainfall intensity can result in substantial flood peaks irrespective of initial soil moisture. Lastly, enhanced flood peaks are associated with relatively low hillslope infiltration and channel roughness (Fig. 5b and 5c).

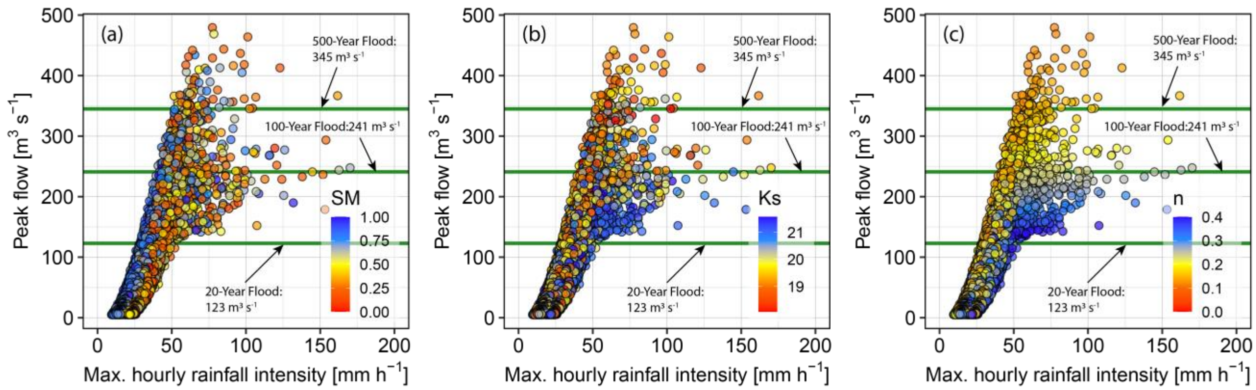

Figure 5. Relationships between CosMoS derived maximum hourly rainfall intensity and K2 model simulated peak flows with respect to (a) watershed antecedent soil moisture, (b) hillslope saturated hydraulic conductivity (K_{sh}), and (c) channel roughness coefficient (n_c).

4.2 Post-wildfire FFA

The deterministic simulations show that the post-wildfire FFA depends on both percentage burn area and in particular time after wildfire (Fig. 6). The difference between the four panels in Fig. 6 can be interpreted as a diminishing role of wildfire in enhancing flood magnitude as the watershed recovers. For instance, the 10-year flood associated with 100% burn area drops from 300 within one year to 150 m^3 s^{-1} two years after wildfire (Fig. 6a and 6b). Within two years after wildfire, flood quantiles for experiments with larger burn areas are consistently higher (Fig. 6a and 6b); differences are negligible for longer post-fire periods. The first-year post-wildfire FFA for 20% to 80% burn area show a step change where the flood magnitude is approximately constant for a range of ARIs (Fig. 6a). Such a phenomena is caused by unburned downstream subwatershed areas and especially the unaffected channels, which act to attenuate the flood waves from the burned areas upstream (Fig. S5 shows two rainfall events of comparable intensity can cause different peakflows due to different wildfire burn locations). However, as rainfall intensity and flood magnitudes increase, the attenuating effects of the unburned downstream subwatersheds diminish. Once flood magnitudes are larger than 50-year events, they increase again with ARI.

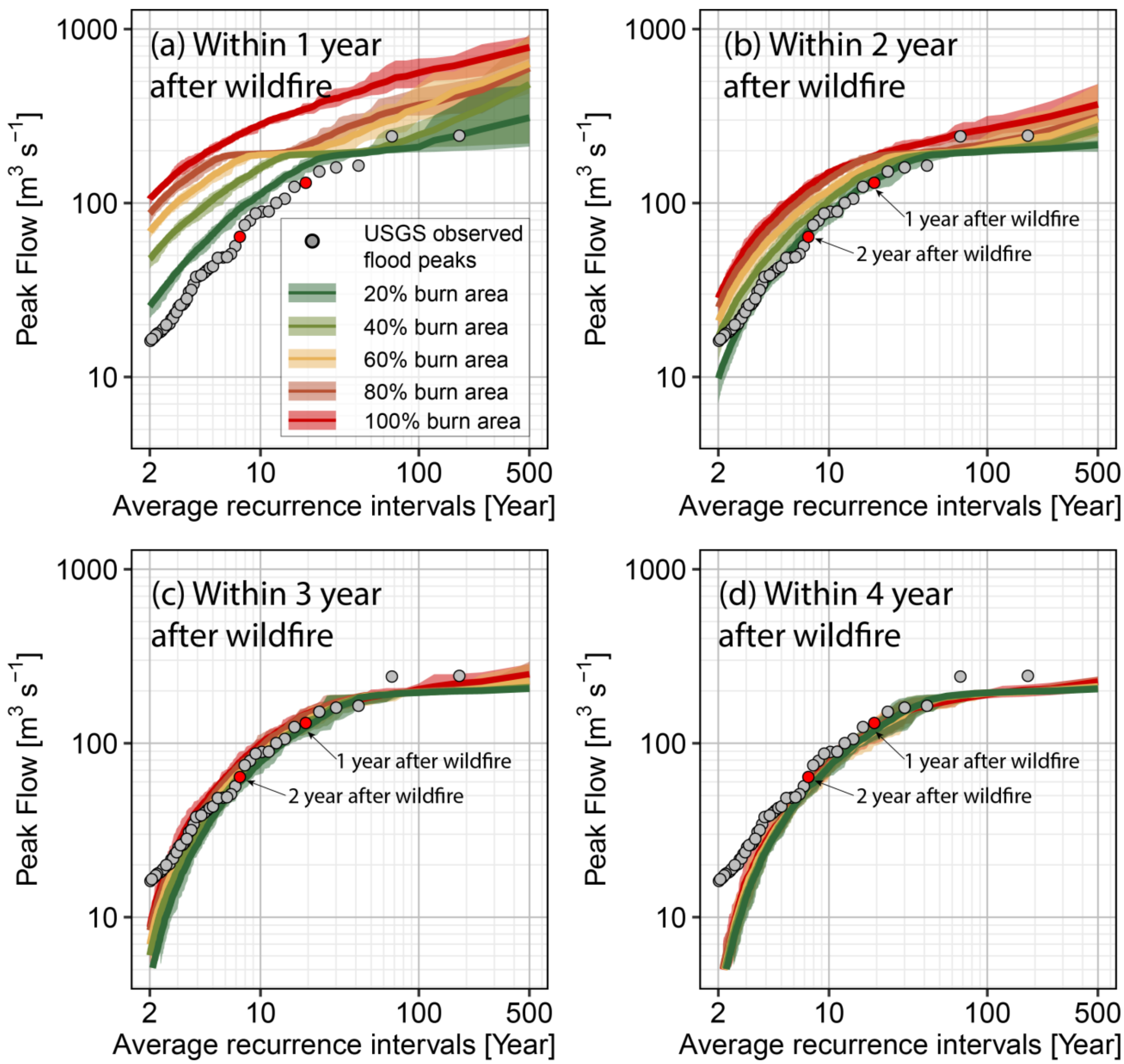

Figure 6. Post-wildfire FFA results with respect to different percent burn area and (a-d) years after wildfire.

4.3 Fire Continuum FFA

Post-wildfire FFA provides flood frequencies only for wildfire-affected periods and thus provide an incorrect picture of the "underlying" long-run flood frequency of the fire-affected watershed. The process-based fire continuum FFA, in contrast, derives the frequencies of floods by calculating the joint probability of rainfall, antecedent watershed soil moisture, occurrence of wildfire, and its impacts and recovery. In this study, the annual probability of M-H wildfire or its reciprocal, wildfire inter-arrival time in years (*T=1/p*), is estimated using the USFS derived M-H wildfire probabilities and a spatial Bootstrap scheme (Section 3.4 and 3.5). The estimated median M-H wildfire recurrence intervals for the uAS watershed corresponds to 63.8 years (Fig. S6), which is similar to the duration between its historical large fires: 64 years between 1896 and the 1959 Woodwardia Fire, followed 51 years later by the 2009 Station Fire. However, this estimated M-H wildfire interval is quite long compared with the ~2-4-year post-fire period during which the flood frequency estimates in Section 4.2 “feel” the burn effects.

Fire continuum FFA resembles pre-wildfire FFA, as well as the USGS observations for ARI smaller than 100 years. Beyond that level, it yields slightly higher estimates than pre-wildfire ones (Fig. 7a). It is significant that fire continuum FFA shows much larger variability than pre-wildfire FFA, especially for ARIs greater than 50 years, indicating a higher potential for more severe floods (Fig. 7a). The difference between pre-wildfire and fire continuum FFA, including the mean and variability, is attributed to the incorporation of wildfire and post-fire recovery into the process-based FFA (Fig. 7a). It must be emphasized that this study does not consider the potential impacts of climate change or land use management on recent or future wildfire occurrences, nor on the length of post-fire recovery periods (see Section 5.3 for further discussion of this limitation).

The 50,000 simulated annual peak flows that constitute the fire continuum FFA results (Fig. 7a) were classified into two categories: fire-affected and non-fire-affected. The former refers to peak flows that occurred within four years of wildfire events, while the latter pertains to peak flows that occurred after that time period. This yields 2,184 (4.4% of the total) and 47,816 (95.6%) fire-affected and non-fire-affected annual peak flows, respectively. Empirical (i.e., using Cunnane plotting positions) distributions as well as 90% confidence intervals for the fire-affected and non-fire-affected peak flows are derived using nonparametric bootstrapping with both sample size and number of repetitions equal to 100 (Fig. 7b and 7c). The empirical distributions for non-fire-affected flood peaks match the USGS observations and pre-wildfire FFA reasonably well (Figs. 4a and 7b). However, the empirical distributions for fire-affected peaks, which represent the combined effects of post-wildfire FFA within four years (Fig. 6), exhibit higher values compared to both USGS observations and pre-wildfire FFA (Fig. 7c).

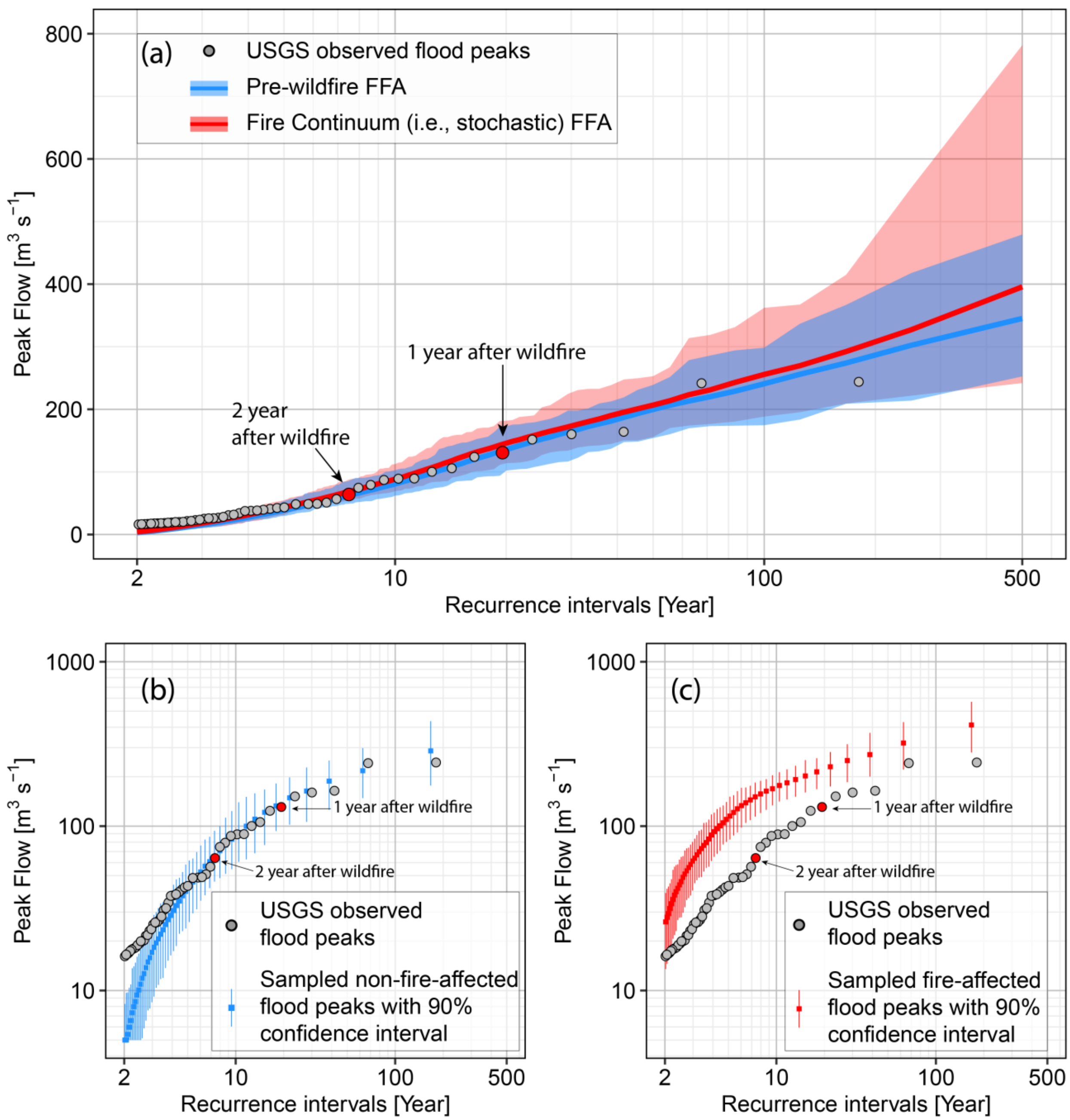

Figure 7. (a) The comparison between pre-wildfire and fire continuum (i.e., stochastic) FFA. 50,000 simulated flood peaks that constitute stochastic FFA are grouped into fire-affected and non-fire-affected, depending on whether they occurred within four years after the simulated wildfire events. Note peak flows in (a) are in linear scale whereas are in log-scale in (b) and (c). Flood peaks within two years after the 2009 Station fire are highlighted in red on all panels.

5 Discussion

5.1 Post-wildfire vs. Fire Continuum FFA

The main objective of our post-wildfire FFA is to examine peak flow distributions in fire-affected years, considered here to be the first four years following fire (Fig. 7c). In other words, the post-wildfire FFA results are conditional distributions because they focus only on specific fire-affected years. In contrast, fire continuum FFA attempts to represent the joint probabilities of rainfall, wildfire occurrence and severity, initial soil moisture, and watershed recovery processes along the synthetic multidecadal timescales (Fig. 7a).

For the uAS watershed, the post-wildfire FFA for 100% burn area and within 1 year after wildfire show pronounced increases across the recurrence intervals: 100-year floods can be three times larger than the pre-wildfire floods (Fig. 6a). While the central tendency of fire continuum FFA results are roughly comparable to the pre-wildfire FFA (i.e., no wildfire effects) due to the long wildfire inter-arrival time (roughly 60 years) compared to the short watershed recovery period (roughly four years), the variability among FFA ensemble members is substantially higher, particularly for rarer flood events (e.g., >100 years). Indeed, the largest 500-year event from our 100-ensemble fire continuum FFA simulations was nearly 800 $m^3 s^{-1}$, while the largest from the pre-fire simulations was less than 500 $m^3 s^{-1}$. These findings suggest that wildfire can have important influences on the upper tail of flood distributions, which is of primary interest in risk management (England et al., 2019; NRC, 1988).

Furthermore, post-wildfire and fire continuum FFA are appropriate tools for reactive and proactive flood risk management, respectively. For recently burned watersheds, post-wildfire FFA can help answer how long post-wildfire flood hazards persist, thus facilitating the evaluation of hazard mitigation strategies. On the other hand, using fire continuum FFA as a proactive estimator can better understand flood risks associated with the potential impacts of wildfires as well as flood and fire mitigation strategies. By doing so, resources can be allocated to locations that have the greatest overall flood hazards, rather than solely focusing on areas that have recently burned. This will facilitate more effective flood risk management and help mitigate potential damage.

5.2 Limitations

As the first effort (to our knowledge) to physically model the impact of wildfire on flood frequency, our study has several limitations. The first and most central is the paucity of streamflow observations during post-wildfire "recovery" periods, which is central to identifying hydrologic changes via inverse modeling approaches. The relatively long (and highly approximate) inter-arrival time of wildfire is problematic enough for the application of inverse modeling in our study basin; application of these techniques to simulate the impacts of wildfire on flood frequencies for ungauged basins is further complicated by uncertainty in the transferability of model parameters designed to represent post-wildfire conditions from one watershed to another (e.g., Canfield et al., 2005; Chen et al., 2013; Ebel & Martin, 2017; Liu et al., 2021). We direct readers to the next subsection for our recommendations on transferring the method employed in this study to other watersheds.

The second limitation pertains to model process representation and performance. We have observed an underestimation in process-based pre-wildfire FFA for common flood events (less than the 3-year event; Fig.4a). This may be because the K2 hydrological model is not designed to represent the saturation excess overland flow resulting from long duration, low intensity rainfall. Similarly, the process-based, pre-wildfire FFA based on K2 simulations may not accurately represent peak flows for extreme events that generate runoff via saturation-excess overland flow, which have been documented in the San Gabriel Mountains (e.g., Doehring, 1968), though there is very good agreement between observations and the pre-fire FFA (Fig.4a; Fig. 7). In addition, saturated hydraulic conductivity and hydraulic roughness are the only two parameters used to represent the hydrological impacts of wildfire in this study and others (e.g., Canfield et al., 2005; Chen et al., 2013).

Third, it is not practical to simulate every potential runoff event to determine the annual peak flow, so we define a criterion (maximum 12-h rainfall total) for selecting the rainfall event that is likely to produce the peak flow in each simulated year. This criterion is based on the time of concentration of the watershed, which likely varies with the time since fire. In addition, annual maximum 15-min and hourly rainfall intensities are comparable with the maximum 15-min and hourly rainfall intensities nested in the annual maximum 12-h rainfall, respectively, based on continuous rainfall intensities of 50,000 synthetic years (Fig. S7).

Lastly, the USFS used current fuel conditions and historical climate data to simulate occurrence and severity of large wildfires for the South Coast climate division. Thus, fire activity in this study does not reflect climate change and its impacts on fuel and vegetation dynamics. As the climate continues to warm, it is expected that fuel will become drier and that drought periods will become longer, resulting in increased wildfire activity and longer periods for vegetation to recover (e.g., Flannigan et al., 2009; Iglesias et al., 2022; Wang et al., 2022). In addition, short duration and high intensity rainfall is projected to increase in future due to climate change (e.g., Easterling et al., 2017; Fowler et al., 2021; Prein et al., 2017).

5.3 Transferability of the Approach

We hypothesize that the impacts of fire on flood magnitude and frequency will vary considerably across hydroclimatic regimes and in different plant communities. Prior studies document a wide range of hydrologic responses following fire, even within the same geographic region (Sheridan et al., 2015). Application of the proposed method in a wider range of settings will help identify patterns and lead to a more comprehensive understanding of the impacts of fire on flooding.

Herein, we provide some recommendations for how the methods shown in this study could be extended to other watersheds. Data availability is a major limiting factor in the transferability of this work. Because post-wildfire floods are sensitive to short-duration, high-intensity rainfall, precipitation data at a high resolution for a relatively long period are necessary. Although soil moisture in this study is derived from a reanalysis dataset, field measurements of soil moisture (especially for post-fire periods) can help indicate watershed recovery. To perform inverse modeling to represent the hydrological impacts of wildfire, instantaneous streamflow measurements for multiple pre- and post-wildfire events are needed. The annual probability of wildfire is available for the CONUS via USFS (Short et al., 2020), but it could potentially be refined with additional local data if available. All these required datasets also highlight the importance of continuously monitoring watershed conditions along the fire continuum.

The second challenge in transferring our method lies in the parameterizations of wildfire impacts and watershed recovery. To determine which soil hydrologic parameters to use for inverse modeling, one must be familiar with the watershed properties and hydrological models that will be used. When the instantaneous streamflow for both pre- and post-wildfire floods are available, one can derive the wildfire-related parameters with respect to time via a set of model calibrations based on Liu et al. (2021).

In locations where post-wildfire streamflow data are not available, two research directions could prove useful. In the short term, regionalization techniques can be used to transfer field-measured, post-wildfire soil hydraulic properties from nearby basins to estimate changes in hydrologic parameters for ungauged basins affected by wildfires (e.g., Ebel & Martin, 2017; Hoch et al., 2021; Perkins et al., 2022; Prats et al., 2021). In the longer term, field-scale studies (e.g., Araya et al., 2017; Parson et al., 2010; Perkins et al., 2022) that investigate the “chain” of processes from wildfire to soil heating and the subsequent effects on soil properties and hydrology offer a promising avenue to establish physically based links between post-wildfire hydrological parameters and wildfire severity.

6 Summary and Conclusions

In this study, we present a process-based FFA framework that integrates a stochastic rainfall generator, wildfire simulation outputs, a physics-based rainfall-runoff model, and model parameters that vary with time after wildfire. Unlike statistical FFA approaches, process-based FFA approaches that simulate a range of flood generating processes show potential for analyzing the complex causal chains of wildfire, hydrologic impacts, and flood frequencies. We used the framework to investigate the cascading effects of wildfire on flood hazard, represented via flood peak flow distributions that account for the transient impacts of wildfire. We applied this framework to the recently-burned uAS watershed in San Gabriel Mountains, Southern California, an area that is affected by extreme post-fire flood and debris-flow activity (e.g., Doehring, 1968; Eaton, 1936; Kean et al., 2011; Palucis et al., 2021). Here, we present five key findings:

1) The process-based, pre-wildfire FFA closely matches USGS observations for moderate to rare events (ARI $\geq$ 3-year; Fig. 4).

2) Process-based results explicitly resolve how different hydrometeorological drivers interact to produce floods: rainfall intensity plays the first-order role in driving flood magnitudes while watershed antecedent soil moisture and channel's roughness can modulate flood peaks (Fig. 5).
3) Post-wildfire FFA for the uAS watershed shows that flood frequencies are dependent on the percentage of watershed area burned and time after wildfire (Fig. 6). The hydrologic impacts of wildfire enhance flood magnitudes across all ARIs for the first two years after wildfire; however, the effects diminish after two years.
4) Fire continuum FFA, which considers both climatological occurrence of wildfires and their interactions with watershed infiltration and channel roughness, antecedent conditions, and rainfall intensity highlights a large increase in the variability of peak flows, especially for the upper tail of peak flow distribution that is of significance for flood risk management.
5) Climatic nonstationarity, though neglected in this study, can exacerbate the compound wildfire-flood hazards by affecting each individual driver (e.g., enhanced rainfall intensity and fire activity) and their interdependency (e.g., the longer vegetation recovery period the larger probability to experience extreme rainfall). Our process-based framework holds the promise to flexibly incorporate understanding of changes in drivers and interdependencies into the simulation of future fire continuum flood frequencies.

Software and Data Availability Statement

The stochastic rainfall generator, CoSMoS can be download from its Github repository via https://github.com/TycheLab/CoSMoS. The K2 hydrological model can be download from US Department of Agriculture via https://www.tucson.ars.ag.gov/kineros/. Precipitation data can be obtained from the Los Angeles County Department of Public Works (https://dpw.lacounty.gov/wrd/Precip). The wildfire burn probability data can be downloaded from US Department of Agriculture, Research Data Archive, via https://www.fs.usda.gov/rds/archive/Catalog/RDS-2016-0034-2.

Acknowledgments

GY's contribution is supported by the Urban Flood Demonstration Program by Department of the Army (Agreement No. W912HZ1920011), which also supports JM, MB (DRI), JG, IF, and MB (U.S. Army Corps of Engineers). TL's and LAM's contributions are supported by the University of Arizona. DBW's and BH's contributions are supported by the University of Wisconsin-Madison and Desert Research Institute, respectively. We thank Nicole Damon at Desert Research Institute for her assistance with technical editing.

References

Abatzoglou, J. T., & Williams, A. P. (2016). Impact of anthropogenic climate change on wildfire across western US forests. *Proceedings of the National Academy of Sciences*, *113*(42), 11770–11775. https://doi.org/10.1073/pnas.1607171113

AghaKouchak, A., Chiang, F., Huning, L. S., Love, C. A., Mallakpour, I., Mazdiyasni, O., et al. (2020). Climate extremes and compound hazards in a warming world. *Annual Review of Earth and Planetary Sciences*, *48*, 519–548.

Albalasmeh, A. A., Berli, M., Shafer, D. S., & Ghezzehei, T. A. (2013). Degradation of moist soil aggregates by rapid temperature rise under low intensity fire. *Plant and Soil*, *362*(1), 335–344.

Alexander, M. E., Cruz, M. G., Alexander, M. E., & Cruz, M. G. (2011). Interdependencies between flame length and fireline intensity in predicting crown fire initiation and crown scorch height. *International Journal of Wildland Fire*, *21*(2), 95–113. https://doi.org/10.1071/WF11001

Araya, S. N., Fogel, M. L., & Berhe, A. A. (2017). Thermal alteration of soil organic matter properties: a systematic study to infer response of Sierra Nevada climosequence soils to forest fires. *SOIL*, *3*(1), 31–44. https://doi.org/10.5194/soil-3-31-2017

Balfour, V. N., Doerr, S. H., & Robichaud, P. R. (2014). The temporal evolution of wildfire ash and implications for post-fire infiltration. *International Journal of Wildland Fire*, *23*(5), 733. https://doi.org/10.1071/WF13159

Barth, N. A., Villarini, G., Nayak, M. A., & White, K. (2017). Mixed populations and annual flood frequency estimates in the western United States: The role of atmospheric rivers. *Water Resources Research*, *53*(1), 257–269. https://doi.org/10.1002/2016WR019064

Bodí, M. B., Martin, D. A., Balfour, V. N., Santín, C., Doerr, S. H., Pereira, P., et al. (2014). Wildland fire ash: Production, composition and eco-hydro-geomorphic effects. *Earth-Science Reviews*, *130*, 103–127. https://doi.org/10.1016/j.earscirev.2013.12.007

Bowman, D. M. J. S., Balch, J. K., Artaxo, P., Bond, W. J., Carlson, J. M., Cochrane, M. A., et al. (2009). Fire in the Earth System. *Science*, *324*(5926), 481–484. https://doi.org/10.1126/science.1163886

Canfield, H. E., Goodrich, D. C., & Burns, I. S. (2005). Selection of Parameters Values to Model Post-Fire Runoff and Sediment Transport at the Watershed Scale in Southwestern Forests. In *Managing Watersheds for Human and Natural Impacts* (pp. 1–12). Williamsburg, Virginia, United States: American Society of Civil Engineers. https://doi.org/10.1061/40763(178)48

Chen, L., Berli, M., & Chief, K. (2013). Examining modeling approaches for the rainfall-runoff process in wildfire-affected watersheds: Using San Dimas Experimental Forest. *JAWRA Journal of the American Water Resources Association*, *49*(4), 851–866.

Cunnane, C. (1978). Unbiased plotting positions — A review. *Journal of Hydrology*, *37*(3), 205–222. https://doi.org/10.1016/0022-1694(78)90017-3

DeBano, L. F. (1981). Water repellent soils: a state-of-the-art. *Gen. Tech. Rep. PSW-46. Berkeley, Calif.: U.S. Department of Agriculture, Forest Service, Pacific Southwest Forest and Range Exp. Stn. 21 p*, *046*. https://doi.org/10.2737/PSW-GTR-46

DeBano, L. F. (2000). The role of fire and soil heating on water repellency in wildland environments: a review. *Journal of Hydrology*, *231–232*, 195–206. https://doi.org/10.1016/S0022-1694(00)00194-3

DiBiase, R. A., & Lamb, M. P. (2019). Dry sediment loading of headwater channels fuels post-wildfire debris flows in bedrock landscapes. *Geology*, *48*(2), 189–193. https://doi.org/10.1130/G46847.1

Doehring, D. O. (1968). The effect of fire on geomorphic processes in the San Gabriel Mountains, California. *Rocky Mountain Geology*, *7*(1), 43–65.

Easterling, D. R., Arnold, J. R., Knutson, T., Kunkel, K. E., LeGrande, A. N., Leung, L. R., et al. (2017). Precipitation change in the United States.

Eaton, E. C. (1936). Flood and Erosion Control Problems and their Solution. *Transactions of the American Society of Civil Engineers*, *101*(1), 1302–1330. https://doi.org/10.1061/TACEAT.0004726

Ebel, B. A. (2012). Wildfire impacts on soil-water retention in the Colorado Front Range, United States. *Water Resources Research*, *48*(12).

Ebel, B. A., & Martin, D. A. (2017). Meta-analysis of field-saturated hydraulic conductivity recovery following wildland fire: Applications for hydrologic model parameterization and resilience assessment. *Hydrological Processes*, *31*(21), 3682–3696. https://doi.org/10.1002/hyp.11288

Ebel, B. A., & Moody, J. A. (2013). Rethinking infiltration in wildfire-affected soils. *Hydrological Processes*, *27*(10), 1510–1514.

England, J. F., Cohn, T. A., Faber, B. A., Stedinger, J. R., Thomas, W. O., Veilleux, A. G., et al. (2019). Guidelines for Determining Flood Flow Frequency–Bulletin 17C (Ver. 1.1, May 2019): US Geological Survey Techniques and Methods, Book 4, Chap. B5. In *United States. Department of the Interior; Geological Survey (US)*. United States. Department of the Interior; Geological Survey (US).

Falcone, J. A. (2011). *GAGES-II: Geospatial attributes of gages for evaluating streamflow*. US Geological Survey.

Finco, M., Quayle, B., Zhang, Y., Lecker, J., Megown, K. A., & Brewer, C. K. (2012). Monitoring Trends and Burn Severity (MTBS): Monitoring wildfire activity for the past quarter century using landsat data. *In: Morin, Randall S.; Liknes, Greg C., Comps. Moving from Status to Trends: Forest Inventory and Analysis (FIA) Symposium 2012; 2012 December*

4-6; Baltimore, MD. Gen. Tech. Rep. NRS-P-105. Newtown Square, PA: U.S. Department of Agriculture, Forest Service, Northern Research Station. [CD-ROM]: 222-228., 222–228.

Finney, M. A., McHugh, C. W., Grenfell, I. C., Riley, K. L., & Short, K. C. (2011). A simulation of probabilistic wildfire risk components for the continental United States. *Stochastic Environmental Research and Risk Assessment*, *25*(7), 973–1000.

Flannigan, M. D., Krawchuk, M. A., de Groot, W. J., Wotton, B. M., & Gowman, L. M. (2009). Implications of changing climate for global wildland fire. *International Journal of Wildland Fire*, *18*(5), 483. https://doi.org/10.1071/WF08187

Florsheim, J. L., Chin, A., Kinoshita, A. M., & Nourbakhshbeidokhti, S. (2017). Effect of storms during drought on post-wildfire recovery of channel sediment dynamics and habitat in the southern California chaparral, USA. *Earth Surface Processes and Landforms*, *42*(10), 1482–1492. https://doi.org/10.1002/esp.4117

Fowler, H. J., Lenderink, G., Prein, A. F., Westra, S., Allan, R. P., Ban, N., et al. (2021). Anthropogenic intensification of short-duration rainfall extremes. *Nature Reviews Earth & Environment*, *2*(2), 107–122. https://doi.org/10.1038/s43017-020-00128-6

García-Corona, R., Benito, E., De Blas, E., & Varela, M. E. (2004). Effects of heating on some soil physical properties related to its hydrological behaviour in two north-western Spanish soils. *International Journal of Wildland Fire*, *13*(2), 195–199.

Goodrich, D. C., Burns, I. S., Unkrich, C. L., Semmens, D. J., Guertin, D. P., Hernandez, M., et al. (2012). KINEROS2/AGWA: Model use, calibration, and validation. *Transactions of the ASABE*, *55*(4), 1561–1574.

Guttman, N. B., & Quayle, R. G. (1996). A historical perspective of US climate divisions. *Bulletin of the American Meteorological Society*, *77*(2), 293–304.

Haas, J. R., Thompson, M., Tillery, A., & Scott, J. H. (2016). Capturing spatiotemporal variation in wildfires for improving postwildfire debris-flow hazard assessments. *Natural Hazard Uncertainty Assessment: Modeling and Decision Support*, 301–317.

Hoch, O. J., McGuire, L. A., Youberg, A. M., & Rengers, F. K. (2021). Hydrogeomorphic Recovery and Temporal Changes in Rainfall Thresholds for Debris Flows Following Wildfire. *Journal of Geophysical Research: Earth Surface*, *126*(12), e2021JF006374. https://doi.org/10.1029/2021JF006374

Hood, S. M., Drury, S., Steelman, T., & Steffens, R. (2020). Proceedings of the Fire Continuum-Preparing for the future of wildland fire; 2018 May 21-24; Missoula, MT. *Proceedings RMRS-P-78. Fort Collins, CO: U.S. Department of Agriculture, Forest Service, Rocky Mountain Research Station. 358 p.*, *78*. Retrieved from https://www.fs.usda.gov/research/treesearch/60581

Iglesias, V., Balch, J. K., & Travis, W. R. (2022). US fires became larger, more frequent, and more widespread in the 2000s. *Science Advances*, *8*(11), eabc0020.

Jian, M., Berli, M., & Ghezzehei, T. A. (2018). Soil structural degradation during low-severity burns. *Geophysical Research Letters*, *45*(11), 5553–5561.

Kean, Jason W., & Staley, D. M. (2021). Forecasting the frequency and magnitude of postfire debris flows across southern California. *Earth's Future*, *9*(3), e2020EF001735.

Kean, Jason W., Staley, D. M., & Cannon, S. H. (2011). In situ measurements of post-fire debris flows in southern California: Comparisons of the timing and magnitude of 24 debris-flow events with rainfall and soil moisture conditions. *Journal of Geophysical Research: Earth Surface*, *116*(F4).

Kean, Jason W., McGuire, L. A., Rengers, F. K., Smith, J. B., & Staley, D. M. (2016). Amplification of postwildfire peak flow by debris. *Geophysical Research Letters*, *43*(16), 8545–8553.

Kean, J.W., Staley, D. M., Lancaster, J. T., Rengers, F. K., Swanson, B. J., Coe, J. A., et al. (2019). Inundation, flow dynamics, and damage in the 9 January 2018 Montecito debris-flow event, California, USA: Opportunities and challenges for post-wildfire risk assessment. *Geosphere*, *15*(4), 1140–1163. https://doi.org/10.1130/GES02048.1

Keeley, J. E. (2009). Fire intensity, fire severity and burn severity: a brief review and suggested usage. *International Journal of Wildland Fire*, *18*(1), 116. https://doi.org/10.1071/WF07049

Kinoshita, A. M., & Hogue, T. S. (2011). Spatial and temporal controls on post-fire hydrologic recovery in Southern California watersheds. *Catena*, *87*(2), 240–252.

Kitzberger, T., Brown, P. M., Heyerdahl, E. K., Swetnam, T. W., & Veblen, T. T. (2007). Contingent Pacific–Atlantic Ocean influence on multicentury wildfire synchrony over western North America. *Proceedings of the National Academy of Sciences*, *104*(2), 543–548. https://doi.org/10.1073/pnas.0606078104

Krammes, J. S. (1960). Erosion from mountain side slopes after fire in southern California. *Research Note (California Forest and Range Experiment Station); No. 171*.

Lamb, M. P., Scheingross, J. S., Amidon, W. H., Swanson, E., & Limaye, A. (2011). A model for fire-induced sediment yield by dry ravel in steep landscapes. *Journal of Geophysical Research: Earth Surface*, *116*(F3). https://doi.org/10.1029/2010JF001878

Lamb, R., Faulkner, D., Wass, P., & Cameron, D. (2016). Have applications of continuous rainfall–runoff simulation realized the vision for process-based flood frequency analysis? *Hydrological Processes*, *30*(14), 2463–2481. https://doi.org/10.1002/hyp.10882

Larsen, I. J., MacDonald, L. H., Brown, E., Rough, D., Welsh, M. J., Pietraszek, J. H., et al. (2009). Causes of post-fire runoff and erosion: Water repellency, cover, or soil sealing? *Soil Science Society of America Journal*, *73*(4), 1393–1407.

Liu, T., McGuire, L. A., Wei, H., Rengers, F. K., Gupta, H., Ji, L., & Goodrich, D. C. (2021). The timing and magnitude of changes to Hortonian overland flow at the watershed scale during the post-fire recovery process. *Hydrological Processes*, *35*(5), e14208.

Liu, T., McGuire, L. A., Oakley, N., & Cannon, F. (2022). Temporal changes in rainfall intensity–duration thresholds for post-wildfire flash floods in southern California. *Natural Hazards and Earth System Sciences*, *22*(2), 361–376. https://doi.org/10.5194/nhess-22-361-2022

Mataix-Solera, J., Cerdà, A., Arcenegui, V., Jordán, A., & Zavala, L. M. (2011). Fire effects on soil aggregation: a review. *Earth-Science Reviews*, *109*(1–2), 44–60.

McGuire, L. A., Rengers, F. K., Kean, J. W., & Staley, D. M. (2017). Debris flow initiation by runoff in a recently burned basin: Is grain-by-grain sediment bulking or en masse failure to blame? *Geophysical Research Letters*, *44*(14), 7310–7319.

McGuire, L. A., Rengers, F. K., Kean, J. W., Staley, D. M., & Mirus, B. B. (2018). Incorporating spatially heterogeneous infiltration capacity into hydrologic models with applications for simulating post-wildfire debris flow initiation. *Hydrological Processes*, *32*(9), 1173–1187. https://doi.org/10.1002/hyp.11458

Moody, J. A., & Ebel, B. A. (2012). Hyper-dry conditions provide new insights into the cause of extreme floods after wildfire. *CATENA*, *93*, 58–63. https://doi.org/10.1016/j.catena.2012.01.006

Napoli, J., Gilbertson-Day, J. W., Scott, J. H., Vogler, K. C., & Brough, A. (2022). A PILOT WILDFIRE RISK ASSESSMENT FOR CALIFORNIA.

NRC. (1988). *Estimating probabilities of extreme floods: methods and recommended research*. National Acad. Press.

Oakley, N. S., Lancaster, J. T., Hatchett, B. J., Stock, J., Ralph, F. M., Roj, S., & Lukashov, S. (2018). A 22-Year Climatology of Cool Season Hourly Precipitation Thresholds Conducive to Shallow Landslides in California. *Earth Interactions*, *22*(14), 1–35. https://doi.org/10.1175/EI-D-17-0029.1

Onda, Y., Dietrich, W. E., & Booker, F. (2008). Evolution of overland flow after a severe forest fire, Point Reyes, California. *Catena*, *72*(1), 13–20.

Palucis, M. C., Ulizio, T. P., & Lamb, M. P. (2021). Debris flow initiation from ravel-filled channel bed failure following wildfire in a bedrock landscape with limited sediment supply. *GSA Bulletin*, *133*(9–10), 2079–2096. https://doi.org/10.1130/B35822.1

Papalexiou, S. M. (2018). Unified theory for stochastic modelling of hydroclimatic processes: Preserving marginal distributions, correlation structures, and intermittency. *Advances in Water Resources*, *115*, 234–252. https://doi.org/10.1016/j.advwatres.2018.02.013

Papalexiou, S. M., Strnad, F., Serinaldi, F., Markonis, Y., & Shook, K. (2020). CoSMoS: Complete Stochastic Modelling Solution.

Parson, A., Robichaud, P. R., Lewis, S. A., Napper, C., & Clark, J. T. (2010). Field guide for mapping post-fire soil burn severity. *Gen. Tech. Rep. RMRS-GTR-243. Fort Collins, CO: U.S. Department of Agriculture, Forest Service, Rocky Mountain Research Station. 49 p., 243*. https://doi.org/10.2737/RMRS-GTR-243

Perica, S., Dietz, S., Heim, S., Hiner, L., Maitaria, K., Martin, D., et al. (2014). NOAA Atlas 14 Precipitation-Frequency Atlas of the United States Volume 6 Version 2.3: California. *US Department of Commerce, National Oceanic and Atmospheric Administration, National Weather Service*, *Silver Spring, Maryland*.

Perkins, J. P., Diaz, C., Corbett, S. C., Cerovski-Darriau, C., Stock, J. D., Prancevic, J. P., et al. (2022). Multi-Stage Soil-Hydraulic Recovery and Limited Ravel Accumulations Following the 2017 Nuns and Tubbs Wildfires in Northern California. *Journal of Geophysical Research: Earth Surface*, *127*(6), e2022JF006591. https://doi.org/10.1029/2022JF006591

Pescaroli, G., & Alexander, D. (2015). A definition of cascading disasters and cascading effects: Going beyond the “toppling dominos” metaphor. *Planet@ Risk*, *3*(1), 58–67.

Prats, S. A., Malvar, M. C., & Wagenbrenner, J. W. (2021). Compaction and cover effects on runoff and erosion in post-fire salvage logged areas in the Valley Fire, California. *Hydrological Processes*, *35*(1), e13997. https://doi.org/10.1002/hyp.13997

Prein, A. F., Rasmussen, R. M., Ikeda, K., Liu, C., Clark, M. P., & Holland, G. J. (2017). The future intensification of hourly precipitation extremes. *Nature Climate Change*, *7*(1), 48–52.

Riaño, D., Chuvieco, E., Ustin, S., Zomer, R., Dennison, P., Roberts, D., & Salas, J. (2002). Assessment of vegetation regeneration after fire through multitemporal analysis of AVIRIS images in the Santa Monica Mountains. *Remote Sensing of Environment*, *79*(1), 60–71.

Rollins, M. G. (2009). LANDFIRE: a nationally consistent vegetation, wildland fire, and fuel assessment. *International Journal of Wildland Fire*, *18*(3), 235–249.

Santi, P., Cannon, S., DeGraff, J., & Shroder, J. (2013). Wildfire and landscape change. *Treatise on Geomorphology*, *13*, 262–287.

Schmidt, K. M., Hanshaw, M. N., Howle, J. F., Kean, J. W., Staley, D. M., Stock, J. D., & Bawdeng, W. (2011). Hydrologic conditions and terrestrial laser scanning of post-firedebris flows in the san gabriel mountains, CA, USA. *Italian Journal of Engineering Geology and Environment*, 583–593.

Scott, J. H. (2005). *Standard Fire Behavior Fuel Models: A Comprehensive Set for Use with Rothermel's Surface Fire Spread Model*. U.S. Department of Agriculture, Forest Service, Rocky Mountain Research Station.

Scott, J. H., Gilbertson-Day, J. W., Moran, C., Dillon, G. K., Short, K. C., & Vogler, K. C. (2020). Wildfire Risk to Communities: Spatial datasets of landscape-wide wildfire risk components for the United States.

Shakesby, R. (2011). Post-wildfire soil erosion in the Mediterranean: Review and future research directions. *Earth-Science Reviews*, *105*(3–4), 71–100.

Shakesby, R., & Doerr, S. (2006). Wildfire as a hydrological and geomorphological agent. *Earth-Science Reviews*, *74*(3–4), 269–307. https://doi.org/10.1016/j.earscirev.2005.10.006

Shakesby, R., Coelho, C. D. A., Ferreira, A. D., Terry, J. P., & Walsh, R. P. (1993). Wildfire impacts on soil-erosion and hydrology in wet Mediterranean forest, Portugal. *International Journal of Wildland Fire*, *3*(2), 95–110.

Sheikholeslami, R., & Razavi, S. (2017). Progressive Latin Hypercube Sampling: An efficient approach for robust sampling-based analysis of environmental models. *Environmental Modelling & Software*, *93*, 109–126. https://doi.org/10.1016/j.envsoft.2017.03.010

Sheridan, G. J., Nyman, P., Langhans, C., Cawson, J., Noske, P. J., Oono, A., et al. (2015). Is aridity a high-order control on the hydro–geomorphic response of burned landscapes? *International Journal of Wildland Fire*, *25*(3), 262–267. https://doi.org/10.1071/WF14079

Short, K. C., Finney, M. A., Vogler, K. C., Scott, J. H., Gilbertson-Day, J. W., & Grenfell, I. C. (2020). Spatial datasets of probabilistic wildfire risk components for the United States (270m) (2nd Edition) [Data set]. Forest Service Research Data Archive. https://doi.org/10.2737/RDS-2016-0034-2

Sivapalan, M., & Samuel, J. M. (2009). Transcending limitations of stationarity and the return period: process-based approach to flood estimation and risk assessment. *Hydrological Processes*, *23*(11), 1671–1675.

Smith, J. A., Villarini, G., & Baeck, M. L. (2011). Mixture Distributions and the Hydroclimatology of Extreme Rainfall and Flooding in the Eastern United States. *Journal of Hydrometeorology*, *12*(2), 294–309. https://doi.org/10.1175/2010JHM1242.1

Smith, R. E., Goodrich, D. C., Woolhiser, D. A., & Unkrich, C. L. (1995). KINEROS-a kinematic runoff and erosion model. *Computer Models of Watershed Hydrology.*, 697–732.

Tang, H., McGuire, L. A., Rengers, F. K., Kean, J. W., Staley, D. M., & Smith, J. B. (2019). Evolution of Debris-Flow Initiation Mechanisms and Sediment Sources During a Sequence of Postwildfire Rainstorms. *Journal of Geophysical Research: Earth Surface*, *124*(6), 1572–1595. https://doi.org/10.1029/2018JF004837

Thomas, M. A., Rengers, F. K., Kean, J. W., McGuire, L. A., Staley, D. M., Barnhart, K. R., & Ebel, B. A. (2021). Postwildfire soil-hydraulic recovery and the persistence of debris flow hazards. *Journal of Geophysical Research: Earth Surface*, *126*(6), e2021JF006091.

Tillery, A. C., & Haas, J. R. (2016). *Potential postwildfire debris-flow hazards—a prewildfire evaluation for the Jemez Mountains, north-central New Mexico*. US Geological Survey.

Tillery, A. C., Haas, J. R., Miller, L. W., Scott, J. H., & Thompson, M. P. (2014). Potential postwildfire debris-flow hazards-a prewildfire evaluation for the Sandia and Manzano Mountains and surrounding areas, Central New Mexico. *Scientific Investigations Report 2014-5161. Reston, VA: US Geological Survey. 24 p.*

Valeron, B., & Meixner, T. (2009). Overland flow generation in chaparral ecosystems: temporal and spatial variability. *Hydrological Processes*, n/a-n/a. https://doi.org/10.1002/hyp.7455

Wang, J. A., Randerson, J. T., Goulden, M. L., Knight, C. A., & Battles, J. J. (2022). Losses of tree cover in California driven by increasing fire disturbance and climate stress. *AGU Advances*, *3*(4), e2021AV000654.

Westerling, A. L., Hidalgo, H. G., Cayan, D. R., & Swetnam, T. W. (2006). Warming and Earlier Spring Increase Western U.S. Forest Wildfire Activity. *Science*, *313*(5789), 940–943. https://doi.org/10.1126/science.1128834

Wright, D. B., Smith, J. A., & Baeck, M. L. (2014). Flood frequency analysis using radar rainfall fields and stochastic storm transposition. *Water Resources Research*, *50*(2), 1592–1615.

Xia, Y., Mitchell, K., Ek, M., Sheffield, J., Cosgrove, B., Wood, E., et al. (2012). Continental-scale water and energy flux analysis and validation for the North American Land Data Assimilation System project phase 2 (NLDAS-2): 1. Intercomparison and application of model products. *Journal of Geophysical Research: Atmospheres*, *117*(D3). https://doi.org/10.1029/2011JD016048

Yu, G., Wright, D. B., Zhu, Z., Smith, C., & Holman, K. D. (2019). Process-based flood frequency analysis in an agricultural watershed exhibiting nonstationary flood seasonality. *Hydrology and Earth System Sciences*, *23*(5), 2225–2243.

Yu, G., Wright, D. B., & Li, Z. (2020). The upper tail of precipitation in convection-permitting regional climate models and their utility in nonstationary rainfall and flood frequency analysis. *Earth's Future*, *8*(10), e2020EF001613.

Yu, G., Wright, D. B., & Holman, K. D. (2021). Connecting Hydrometeorological Processes to Low-Probability Floods in the Mountainous Colorado Front Range. *Water Resources Research*, *57*(4), e2021WR029768.

Yu, G., Wright, D. B., & Davenport, F. V. (2022). Diverse Physical Processes Drive Upper-Tail Flood Quantiles in the US Mountain West. *Geophysical Research Letters*, e2022GL098855.

Yu, G., Miller, J., & Sachiko, S. (2022). *Wildfire Impacts on Annual Flood Peaks Across the Western United States* (Technical Report No. 41291) (p. 24). Las Vegas, NV: Desert Research Institute.

Zhu, Z., Wright, D. B., & Yu, G. (2018). The impact of rainfall space-time structure in flood frequency analysis. *Water Resources Research*, *54*(11), 8983–8998.

Zscheischler, J., Westra, S., van den Hurk, B. J. J. M., Seneviratne, S. I., Ward, P. J., Pitman, A., et al. (2018). Future climate risk from compound events. *Nature Climate Change*, *8*(6), 469–477. https://doi.org/10.1038/s41558-018-0156-3

Zscheischler, J., Martius, O., Westra, S., Bevacqua, E., Raymond, C., Horton, R. M., et al. (2020). A typology of compound weather and climate events. *Nature Reviews Earth & Environment*, *1*(7), 333–347.